Research Article Vol. 37, No. 11 / November 2020 / Journal of the Optical Society of America A C95

Journal of the Optical Society of America A

OPTICS, IMAGE SCIENCE, AND VISION

Frequency stability characterization: DFB laser and Raman pump performance on a distributed clock signal over 24.69 km fiber

D. M. Osiemo,[1,*] D. W. Waswa,[1] K. M. Muguro,[1] G. M. Isoe,[2] T. B. Gibbon,[2] and A. W. R. Leitch[2]

[1]Optical Fibre and Laser Research Group, University of Eldoret, P.O. Box 1125, Eldoret, 30100, Kenya
[2]Centre for Broadband Communication, Nelson Mandela University, P.O. Box 77000, Port Elizabeth, 6031, South Africa
*Corresponding author: douglasosiemo@yahoo.com

Received 26 May 2020; revised 14 July 2020; accepted 21 July 2020; posted 21 July 2020 (Doc. ID 396738); published 20 August 2020

Distribution of timing and frequency signals in a fast-changing world requires unprecedented levels of stability for characterization. Transfer of frequency references over long distance without introducing any additional instability is of urgent concern for optical clock development. Choice of optical transmitter is critical to achieving accurate and stable RF clocks for end users. In this paper, we report the stability performance of the distributed feedback (DFB) laser and the Raman pump for transmitted clock signals. The DFB laser and the Raman pump were modulated with 2, 4, and 6 GHz RF clock signals from a signal generator and transmitted over 24.69 km SMF-Reach fiber. At 10 kHz offset frequency, we measured lowest phase noise of −121.22 dBc/Hz and highest spectra power of −5.38 dBm at 2 GHz for the DFB laser. Transfer stabilities of 1.366×10^{-12} and 1.626×10^{-12} for 2 and 4 GHz, respectively, at 1000 s averaging time were achieved. This technique does not require additional amplifiers for long-distance frequency distribution, making it simple and economical, and hence satisfying the requirements for next-generation optical fiber networks.

https://doi.org/10.1364/JOSAA.396738

1. INTRODUCTION

Stable frequency sources play an important role in modern metrology and fundamental physics applications. High sensitivity is required in transmission systems, and thus low noise and stable oscillators and clocks are employed. However, optical transmitters, receivers, and passive components add some instabilities that degrade system performance, resulting in instabilities in the system. Demand for a cost-effective and simple system for distributing stable reference frequency is being explored. A challenge in the distribution of coherent frequency sources is how to transmit a coherent signal over long distances with minimal perturbation. The traditional solutions for long-haul time and frequency (T&F) transfer are based on satellite techniques that use either global navigation satellite systems (GNSS) or geostationary satellites [1–3]. This method is used to compare the frequency and time standards of national laboratories around the world. In this scheme, both the transmitter and receiver compare their times simultaneously with that of a common global positioning satellite (GPS) that is in view of both. The satellite T&F transfer is widely accessible but does not allow one to exploit the actual accuracy and stability of the best atomic clocks and timescales at the remote end. Considering the complexity and cost, it is desirable to implement frequency transfer over the existing widespread fiber-optic telecom networks. An optical fiber is a promising alternative for stable distribution of a frequency reference. The frequency reference, either optical or microwave, is encoded onto an optical carrier for transmission over a fiber network. Remote users are then able to recover the frequency reference by decoding the received optical signal. It has been shown that optical fiber has the potential to disseminate stable radio-frequency (rf) signal over long distance due to its low attenuation, high reliability, and immunity to electromagnetic interference [4,5]. The Jet Propulsion Laboratory paved the way for the development of a fiber-based distribution system for the NASA Deep Space Network [6–8]. In astronomy, modern telescope synchronization such as that at the Atacama Large Microwave Array (ALMA) relied on optical fiber for transmission [9], while the National Institute for Standard and Technology (NIST) has been connected with JILA using a high-performance optical link [10].

Optical fiber also provides a means for remote comparison between highly accurate time and optical-frequency standards, for example, transfer of repetition rate of highly stable mode-locked laser pulses [11], comparisons of optical clock over a 920 km fiber link [12], and a 540 km fiber-optic network carrying internet traffic [13,14]. Continuous frequency transfer

with an accuracy of 5×10^{-19}/day over an 80 km fiber link and stability of 2.43×10^{-12}/s for freely running fiber has also been reported [15]. In other studies, transfer of a clock signal together with data traffic has been reported [16,17], using a high-gain amplifier for a long-haul link. Transfer solution of RF reference signal at 10 and 100 MHz has been proposed [13,18]. Moreover, optical carrier transfer techniques have been developed to observe the relative frequency stability of optical clocks and cavity-stabilized lasers [19,20]. Advancements in semiconductor lasers and receiver technologies have led to adoption of VCSELs in reference frequency (RF) distribution systems [21–23]. Time and reference transfer using VCSEL-based Raman technology for extended reach has been reported [24]. Recently, we presented a real-time technique for transmitting accurate data and a stable clock signal for long-reach optical networks employing a Raman pump to transmit RF clock [25]. For RF modulated frequency dissemination, the laser carrier should have large spectral width. In fiber-optic communication, transfer distance at a certain data rate is often given by a laser's dispersion tolerance. Low modulation frequency leads to longer transfer distance, but such systems but cannot achieve high dissemination stability due to their low phase resolution [26]. Consequently, for longer distance, cascaded frequency dissemination is the best choice, meaning disseminated frequency has to be demodulated and remodulated again using a cascaded frequency stabilization system. Long-term continuous frequency dissemination which give stability at the integration time of 10^6 s has been reported using only an RF modulated frequency-dissemination method [27]. Furthermore, the introduction of a system that simultaneously transmits stable RF signal and data is a novel technology in transmission systems. The development of long-distance, high-resolution frequency transfer is an important issue in remote clock synchronization and comparison [28]. Long baseline interferometers [29] and deep space networks [30] in astrophysics benefit from such a frequency transfer system. Performance of VCSEL and DFB lasers on 1 and 10 kHz clock signals has been investigated [31]. Wavelength shifting of a modulated laser is one of the main factors limiting long-term stability of time and frequency output signals [32]. There is need to investigate noise contribution by high-power transmitters for a clock dissemination system. This will lead to the evolution of new systems that satisfy frequency users' demands.

2. STRUCTURES FOR THE DFB LASER AND THE RAMAN PUMP

Figure 1 shows the structure of a distributed feedback (DFB) laser. DFB lasers employ Bragg diffraction gratings in the active gain region of the semiconductor to form a waveguide [33,34]. Light travelling in the active layer move in all directions, and so will eventually strike the upper surface of the active layer. In this way, the corrugations act as a grating, reflecting only a specific wavelength back into the cavity but allowing others to pass through. The desired wavelength is fed back into the cavity, and this takes place over the whole length of the laser, thereby achieving the distributed feedback. In DFB lasers, one axial resonator mode prevails over the other modes. This yields a relatively narrow single-mode emission peak at the desired

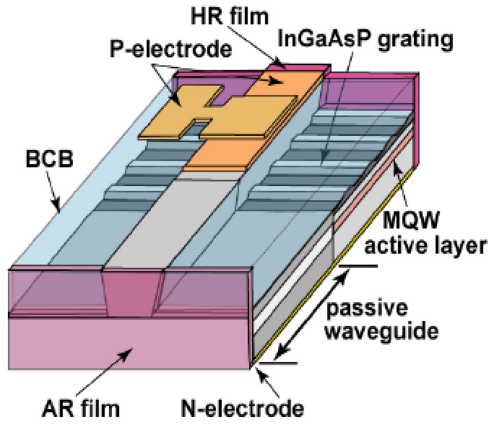

Fig. 1. Structure of the DFB laser (Ref. [37]).

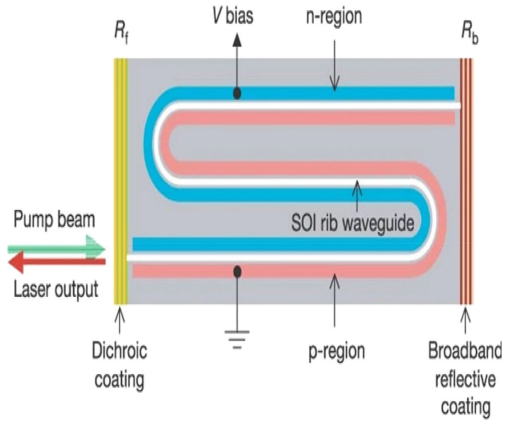

Fig. 2. Schematic diagram showing the structure of the CW Raman laser (Ref. [39]).

wavelength. Commercial DFB lasers have a typical linewidth of 1–10 MHz. Narrow-linewidth laser sources are useful for many diverse applications, including coherent communication, stable frequency standards, nonlinear optics, and precision sensing [35,36].

The oscillation wavelength of the DFB laser is determined mainly by the equivalent refractive index of the grating region and the grating pitch [38]. The grating applied to the DFB laser is formed by electron beam lithography or laser interference lithography, etching, and subsequent planar buried growth [37]. The top view structure for the CW Raman laser is shown in Fig. 2. The light is confined in the S-shaped waveguide formed using a silicon-on-insulator (SOI) structure. The intrinsic (i) Si layer in the p-i-n structure guides the light. External bias is applied to the p and n layers surrounding the intrinsic layer on its two sides.

Stimulated Raman scattering (SRS) and amplification take place in the S-shaped region labeled SOI rib waveguide. The actual material (SOI) is intrinsic silicon surrounded by two p- and n-type regions of Si on its two sides and a layer of silicon oxide (insulator) beneath it [39,40]. There are three essential components in a laser:

a. an active medium in which amplification of the lightwave takes place due to stimulated emission,
b. a mechanism to provide positive feedback to amplified radiation to enable emission of self-sustained oscillation, and
c. a pump source which lifts the electrons from the ground state to an excited state to create population inversion between the excited and ground states.

The active Si region in which SRS occurs is surrounded on its two sides by lower refractive index p- and n-type silicon [40]. Light is then confined in the higher-index Si region, much in the same manner as light is guided in the core of an optical fiber. The two plane parallel mirrors, R_f and R_b, provide the feedback. The emission of Stokes radiation is quite feeble for low pump power. However, as the pump power exceeds a threshold, stimulated process dominates and as a result, the Stokes intensity increases rapidly with an increase in pump power. This pump laser is still an optically pumped source. However, in all applications related to electronics, computer and communication, it is necessary that the control be by an external electrical bias [40].

Phase stability is characterized by the spectral linewidth of the light source. The fundamental linewidth limit of most lasers originates from the spontaneous emission coupled to the lasing mode [36,41]. Stimulated emission, which provides the gain in lasers, is inevitably accompanied by spontaneous emission, which introduces phase noise by combining incoherently with the laser field. The linewidth of a laser decreases with a decreased spontaneous emission rate into the lasing mode and with an increasing number of photons stored in the cavity. The laser linewidth is indeed a crucial parameter for optical fiber telecommunication systems, as it obviously impacts the purity of the signal phase, as well as the intensity noise at the optical receiver.

3. MEASUREMENT OF FREQUENCY STABILITY AND PHASE NOISE

The frequency accuracy of an oscillator is the offset from the specified target frequency while frequency stability is the spread of the measured oscillator frequency about its operational frequency in a period of time. Stability indicates how well an oscillator can produce the same time or frequency offset over a given time interval. Short-term stability refers to fluctuations over intervals less than 100 s, and is due to instantaneous frequency variation around a nominal center frequency. Long-term stability can refer to measurement intervals greater than 100 s, but usually refers to periods longer than one day and is caused by a change in average or nominal center frequency. Figure 3 shows the accuracy and stability examples for a frequency source. There are two classes of characterization of the instability of a frequency source. The first method is phase noise measurement, which is generally considered as the short-term phase/frequency fluctuation of an oscillator or other RF/microwave component due to different noise sources. Phase noise is a method of characterizing the stability of a frequency source, and is done by directly measuring phase fluctuations. Phase noise is useful for determining the short-term stability of the signal that is to be used for synchronization of various system components. The second method involves determining how the measured

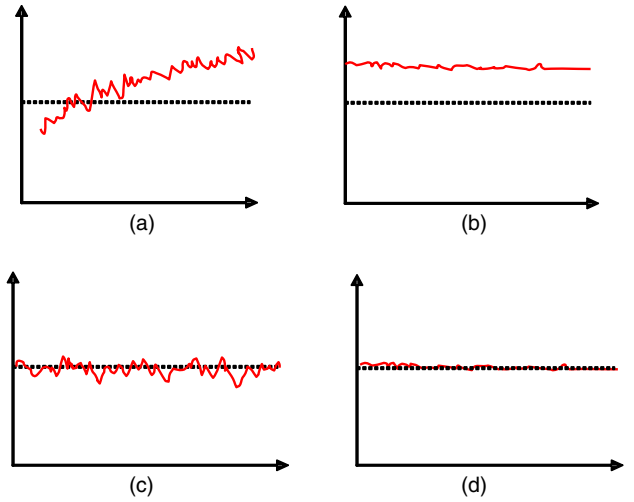

Fig. 3. Relationship between stability and accuracy (Ref. [42]): (a) unstable and not accurate, (b) stable but not accurate, (c) accurate but not stable, and (d) stable and accurate.

fractional frequency fluctuations of the source vary as a function of the time over which the frequency is averaged, and is commonly expressed using the Allan deviation. Allan deviation is the most common statistical function used to characterize and classify frequency fluctuations of a frequency reference. It overcomes convergence and non-stationarity difficulties that might appear for some phase noise cases. Allan deviation $\sigma_y(\tau)$ can be computed from a series of consecutive frequency measurements, each obtained by averaging over a period of time τ. This averaging time corresponds to the gate time of a frequency counter used to make the frequency measurements [43,44]. The Allan deviation for averaging time is defined as

$$\sigma_y(\tau) = \left\langle \frac{1}{2}\left[\bar{y}(t+\tau) - \bar{y}(t)\right]^2 \right\rangle^{1/2}, \tag{1}$$

where $\langle\rangle$ indicates an infinite time average and $\bar{y}$ represents the time average of $y(t)$ over a period τ. $\sigma_y(\tau)$ can be estimated from a finite set of N consecutive average values of the center frequency, v_i, each averaged over a period τ:

$$\sigma_y(\tau) = \left[\frac{1}{2(N-1)v_0^2} \sum_{i=1}^{N-1} (\bar{v}_i - \bar{v}_{i+1}) \right]^{1/2}. \tag{2}$$

An Allan deviation graph shows that the stability of the device improves as the averaging period gets longer since some noise types can be removed by averaging. At some point, however, more averaging no longer improves the results. This point is the noise floor, or the point where the remaining noise consists of a non-stationary processes such as flicker noise or random walk. Five noise types in the time and frequency are white phase, flicker phase, white frequency, flicker frequency, and random walk frequency [43,45]. In this paper, we present a method that distributes reference frequency using existing optical fiber communication networks. Both short-term and long-term stability measurement are done for the distributed clock signals.

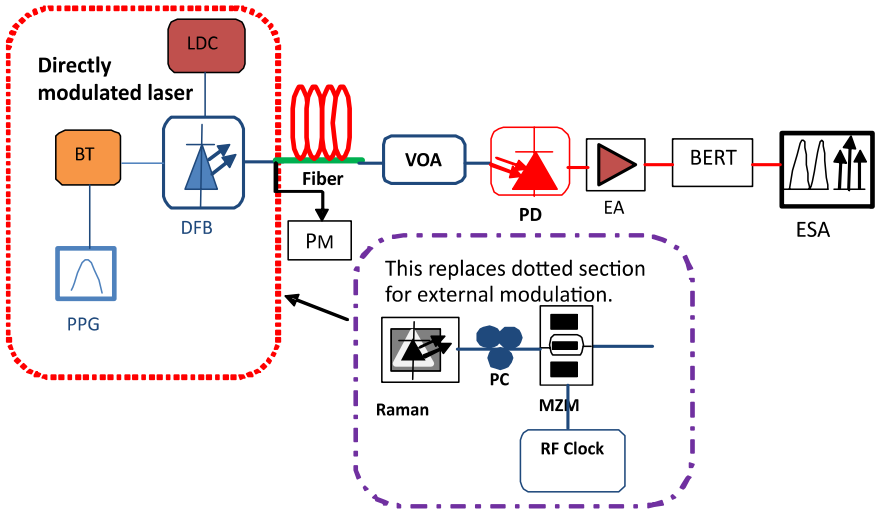

Fig. 4. Experimental setup for RF clock signal dissemination using a modulated DFB laser and a Raman pump. PM, power meter; BT, bias tee; PPG, programmable pattern generator; LDC, laser diode controller; DFB, distributed feedback laser; PC, polarization controller; MZM, Mach–Zehnder modulator; ATT, attenuator; PD, photo diode; EA, electrical amplifier; ESA, electrical spectrum analyzer.

4. EXPERIMENTAL SETUP

Figure 4 shows the experimental setup used to demonstrate different RF clock signal disseminations over 24.69 km standard single-mode fiber (SMF). A 1550 nm DFB laser was directly modulated with 2, 4, and 6 GHz RF clock signals from a signal generator and distributed over 24.69 km fiber. The bias tee (BT) combined the laser diode controller with programmable pattern generator to directly modulate the DFB laser. We optimized the DFB laser by varying bias current from 0.05 to 99.05 mA and output power measured by a power meter (PM). Performance of a 1450 nm Raman pump in clock distribution was then done by externally modulating the laser with RF clock from the signal generator. The resultant electrical signal after the PD was measured with frequency counter-resolution of 100 MHz and analyzed with electrical spectrum analyzer (ESA). The transmitted signal was recovered by a PD and the phase noise measured directly using ESA. We measured long-term stability of the RF signal using a computer based on Rodhe & Schwarz (R&S) Allan variance software.

Frequency stability of the transmitted signal along a 24.69 km link is experimentally evaluated and presented. Performance of a DFB-laser-generated optical clock was compared to that of a Raman pump as a way of carefully designing the transmission link and choosing components that reduce noise contributions affecting clock stability.

5. RESULTS AND DISCUSSION

A. Stability of Clock Signal

Stability results for the DFB laser and the Raman pump are presented in this section. Before choosing a laser for any optical communication system, characterization is important to determine the optimum working of the laser. Figure 5 shows the optimization results of the considered 1550 nm DFB laser. As shown in Fig. 5, a threshold current of 11.0 mA was attained for the DFB laser. The inset of Fig. 5 shows a spectrum for the DFB

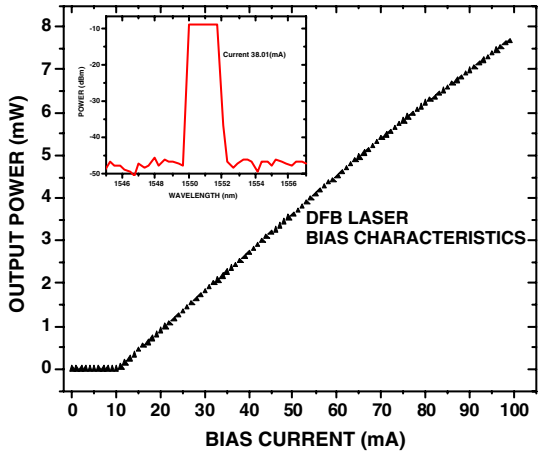

Fig. 5. Variation of output power with DFB bias current-lasing spectra at tuning currents from 0.05 to 99.05 mA. Inset: lasing spectrum for DFB laser at 38.01 mA.

at 38.01 mA. The DFB laser cannot be tuned to a higher wavelength by increasing bias current like VCSEL lasers [25,31]. For optimum performance, we chose bias current above the threshold that is 38.01 mA for the rest of the experiments involving the DFB laser. Accurate and precise synchronized time and frequency distribution is key to optical communication networks. High-speed data transport requires the use of optical fibers for timing frequency signals as well for data transfer.

A 24.69 km optical fiber was used to distribute optical signal and the effect it has on the phase stability of the clock studied extensively. Figures 6(a)–6(c) show results for back to back (B2B), the DFB laser, and the Raman pump at 2, 4, and 6 GHz RF clock signal. Peak powers for B2B, the DFB laser, and the Raman pump at 2 GHz are 5.11, −5.79, and −33.90 dBm, respectively, while at 4 GHz we have 4.74, −8.34, and −37.58 dBm, respectively. Finally, peak powers for B2B, the DFB laser, and the Raman pump at 6 GHz are

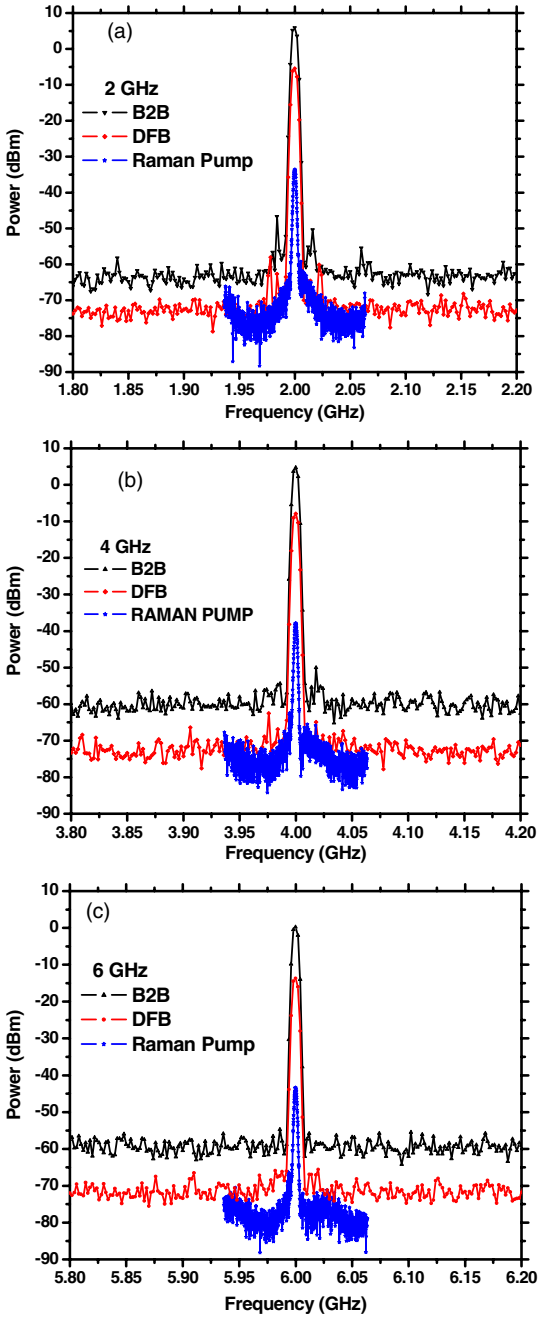

Fig. 6. (a) Spectra for B2B, the DFB laser, and the Raman pump at 2 GHz clock signal. (b) Spectra for B2B, the DFB laser, and the Raman pump at 4 GHz clock signal. (c) Spectra for B2B, the DFB laser, and the Raman pump at 6 GHz clock signal.

0.882, −13.569, and −42.47 dBm, respectively. As shown in Fig. 6, spectrum peak power decreases with an increase in RF frequency. Increasing RF clock frequency peak powers reduces because noise sidebands are created on the carrier frequency, thus weakening the power in the carrier by spreading it into the sidebands. B2B peak powers for 2, 4, and 6 GHz RF frequencies are higher than those for fiber transmission. This is attributed to fiber impairments like dispersion, which is a function of fiber length. Note that in fiber transfer, mechanical perturbations to the transfer path will influence the fractional instability at a level independent of the carrier frequency. Carrier frequency instability is expressed by averaging carrier frequency and then measuring the power at various offsets from the carrier frequency in a defined bandwidth. It is noted that the peak powers for the DFB laser at all RF clock frequencies is higher than that of the Raman pump laser, an indication that DFB is suitable for transmitting clock signals over long distance. Different lasers affect signal central power which affects phase noise.

The directly modulated lasers show a higher output than that of the externally modulated source. The weak RF power available means that electronic amplification must be applied in order to drive subsequent RF circuitry for phase detection without accumulating a significant amount of additional noise.

B. Phase Noise Measurement

By measuring the total carrier power and then measuring the noise signal at a specified offset from the carrier, phase noise measurement can be derived. Phase noise results from frequency variation around the nominal central frequency. Figure 7 shows phase noise evolution as a function of offset frequency. As shown in Fig. 7(a) the phase noise at offset frequency of 10 kHz for B2B at 2, 4, and 6 GHz are −120.27, −114.94, and −111.66 dBc/Hz, respectively. Meanwhile, Fig. 7(b) shows the sideband phase noise curve for 24.69 km fiber transmission using the DFB laser and the Raman pump. The phase noise measured values for the DFB laser at offset frequency of 10 kHz at 2, 4, and 6 GHz are −119.93, −114.42, and −111.21 dBc/Hz, respectively, while for the Raman pump, phase noise measured values are −102.50, −101.58, and −96.54 dBc/Hz, respectively. Phase noise is observed to increase as RF frequency increases to a higher value. The 24.69 km fiber transmission introduces some instability to the transmitted signal, resulting in increase in phase noise, and is severe for longer fibers. Noise may come from internal reflections at fiber interconnects and polarization mode dispersion (PMD) fluctuations. For all frequencies used, we see similar noise characteristics. Phase noise performance profile changes with increasing offset frequency. As observed in Fig. 7(b), RF clock of 6 GHz showed the highest phase noise. This is mainly due to much noise, which degrades the transmitted clock signal by perturbing its phase. Different characteristics of regions are observed on single side band (SSB) phase noise plot. The regions arise from different sources of oscillator noise contribution. Very close to the carrier frequency, random noise is predominant. This noise usually relates to the oscillator physical working environment. If the oscillator is affected by mechanical shocks, vibration, temperature, or other environmental effects, then random noise will remarkably increase close to the carrier frequency. Flicker noise was seen to dominate between 1 Hz and 10 kHz. Flicker phase noise may be related to the physical resonance mechanism of an oscillator or choice of parts used for the electronics design of the oscillator, but it is usually added by noisy electronics. However, flicker phase noise may be minimized by a quality low-noise amplifier design and other electronic components.

White phase noise, on the other hand, is a broadband phase noise and has little to do with the resonance mechanism. Different stages of amplification are usually responsible for

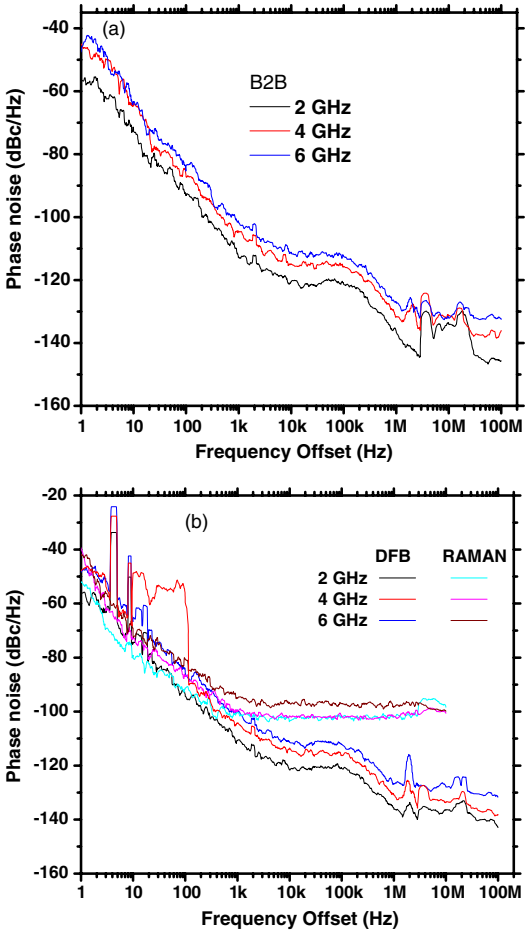

Fig. 7. (a) SSB phase noise evolution with offset frequency for B2B. (b) Evolution of SSB phase noise with offset frequency at 2, 4, and 6 GHz for the DFB laser and the Raman pump.

white noise accumulation. It can be minimized through good quality amplifier design or increasing power of the primary frequency source to avoid unnecessary amplification. For all RF clocks used, phase noise for the DFB laser is lower than that of the Raman pump. However, the phase noise curve for the Raman pump is generally smooth, and hence more stable than the DFB laser. At offset frequency below 500 Hz, DFB suffers from higher phase fluctuations that will dramatically degrade the system performance. The difference in performance for the two lasers may be attributed to differences in the structural designs, semiconductor material, and operating specifications. The DFB laser has the highest peak power and best noise performance, with the lowest phase noise of −118.65 dBc/Hz at 10 kHz offset frequency. Consequently, using the DFB transmitter for frequency distribution results in a simple and economical method that will satisfy a remote frequency user's demands. Potential users are laboratories involved in clock/oscillator development, high-resolution spectroscopy, radio astronomy observations, and relativistic geodesy.

C. Allan Deviation

Allan deviation is useful for characterizing a frequency source because the type of phase noise present is revealed by the way in

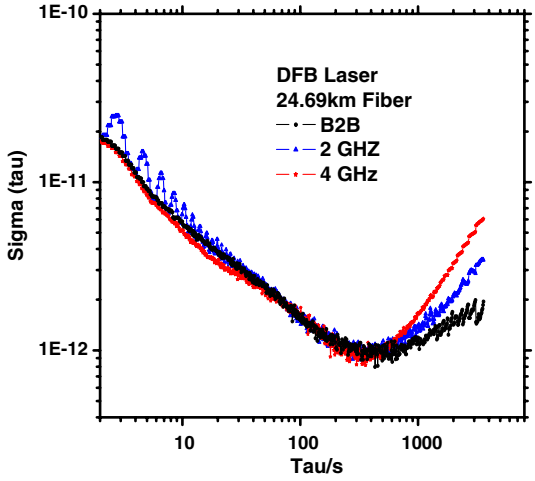

Fig. 8. Log–log plot of Allan deviation as a function of averaging time for B2B, 2 GHz, and 4 GHz RF clock.

which $\sigma_y(\tau)$ depends on τ. Allan deviation (long-term stability) was experimentally demonstrated only for 2 and 4 GHz RF frequency using the DFB laser as the transmitter. The long-term stability measurement of the RF clock signal was analyzed using Allan deviation. Figure 8 shows the log–log plot of Allan deviation as a function of averaging time (sigma tau) for B2B and 24 km fiber using the DFB laser. At 1000 s averaging time, Allan deviation obtained for B2B is 1.166×10^{-12}. After 24.69 km fiber transmission, Allan deviation of 1.366×10^{-12} and 1.626×10^{-12} was obtained for 2 and 4 GHz modulation frequency at the 1000 s averaging time. Figure 8 shows that stability of the device improves as averaging period gets longer since some noise types can be removed by averaging. At the noise floor, however, more averaging no longer improves the results. The stability curve also showed different slopes implying different noise sources cumulatively, contributing to the overall instability of the RF signal. Noise contribution over the first 100 s of averaging time was different from noise contribution after the first 100 s. This is seen with different gradients experienced between the two averaging time regions. At the first 100 s of the resultant spectra, band overlap was noted to decrease with an increase in modulation RF clock frequency. For time scale above 1000 s, the frequency stability is mainly restricted by the electronic components' temperature sensitivity in the phase compensation feedback network. For long averaging, the slope decreases, which is attributed mainly to temperature fluctuations of the small residual uncompensated fibers. Allan deviation is useful in characterizing a frequency source since the type of phase noise present is revealed by how it depends on the period.

6. CONCLUSION

To enhance stability, time and frequency reference systems require the proper choice of laser and appropriate modulation levels. We have experimentally demonstrated 2, 4, and 6 GHz clock transmission over 24.69 km of optical fiber. The DFB laser and the Raman pump were successfully utilized to transmit clock signals, which are important in timing applications.

At 10 kHz offset frequency, the DFB laser recorded lowest phase noise of −121.22 dBc/Hz and highest spectra power of −5.38 dBm at 2 GHz for 24.69 km fiber link. The experimentally assessed stability of the demonstrated transfer system is 1.047×10^{-12} and 1.626×10^{-12} for 2 and 4 GHz, respectively, at 1000 s averaging time for the DFB laser. Stability of the signal depends on averaging time. For averaging time less than 10 s, the 2 GHz clock suffers from periodic fluctuations. This can be attributed to some periodic instability such as environmental sensitivity, which has a direct influence on clock stability. At higher averaging time, stability profile is not as per inherent characteristics of frequency source, indicating non-stationary behavior of the source. Using a DFB laser promotes high stability in the optical carrier and uncertainty of time transfer. Our experimental demonstration shows that it is possible to transfer optical frequency over long distances in optical fiber with high frequency stability.

Funding. National Commission for Science, Technology and Innovation; African Laser Centre, Council for Scientific and Industrial Research (LHIP500 task ALC-R001).

Acknowledgment. We thank Centre for Broadband Communication, Nelson Mandela University, for the use of their laboratory.

Disclosures. The authors declare no conflicts of interest.

REFERENCES

1. W. Lewandowski, J. Azoubib, and W. J. Klepczynski, "GPS: primary tool for time transfer," Proc. IEEE **87**, 163–172 (1999).
2. G. Petit and Z. Jiang, "GPS all in view time transfer for TAI computation," Metrologia **45**, 35–45 (2008).
3. D. Piester, A. Bauch, L. Breakiron, D. Matsakis, B. Blanzano, and O. Koudelka, "Time transfer with nanosecond accuracy for the realization of international atomic time," Metrologia **45**, 185–198 (2008).
4. S. M. Foreman, K. W. Holman, D. D. Hudson, D. J. Jones, and J. Ye, "Remote transfer of ultrastable frequency references via fiber networks," Rev. Sci. Instrum. **78**, 021101 (2007).
5. F. Narbonneau, M. Lours, S. Bize, A. Clairon, G. Santarelli, O. Lopez, Ch. Daussy, A. Amy Klein, and Ch. Chardonnet, "High resolution frequency standard dissemination via optical fibre metropolitan network," Rev. Sci. Instrum. **77**, 064701 (2006).
6. L. Primas, G. Lutes, and R. Sydnor, "Fibre optic frequency transfer link," in *Proceedings of the 42nd Annual Symposium on Frequency Control* (1988), pp. 478–484.
7. E. Lori, L. Primas, T. Ronald, R. T. Logan, and G. F. Lutes, "Applications of ultra-stable fibre optic distribution systems," in *Proceedings of the 43rd Annual Symposium on Frequency Control* (1989), pp. 202–211.
8. R. T. Logan and G. F. Lutes, "High stability microwave fibre optic systems: demonstrations and applications," in *Proceedings of the 43rd Annual Symposium on Frequency Control* (1992), pp. 310–316.
9. K. Sato, T. Hara, S. Kuji, K. Asari, and M. Nishio, "Development of an ultrastable fibre optic frequency distribution system using an optical delay control module," IEEE Trans. Instrum. Meas. **49**, 19–24 (2000).
10. K. W. Holman, D. J. Jones, D. D. Hudson, and J. Ye, "Precise frequency transfer through a fibre network using 1.5-μm mode-locked sources," Opt. Lett. **29**, 1554–1556 (2004).
11. G. Marra, H. S. Margolis, and D. J. Richardson, "Dissemination of an optical frequency comb over fibre with 3×10^{-18} fractional accuracy," Opt. Express **20**, 1775–1782 (2012).
12. K. Predehl, G. Grosche, S. M. F. Raupach, S. Droste, O. Terra, J. Alnis, Th. Legero, T. W. Hänsch, Th. Udem, R. Holzwarth, and H. Schnatz, "A 920-kilometer optical fibre link for frequency metrology at the 19th decimal place," Science **336**, 441–444 (2012).
13. O. Lopez, A. Haboucha, B. Chanteau, C. Chardonnet, A. Amy-Klein, and G. Santarelli, "Ultra-stable long distance optical frequency distribution using the internet fibre network," Opt. Express **20**, 23518–23526 (2012).
14. O. Lopez, A. Kanj, P.-E. Pottie, D. Rovera, J. Achkar, C. Chardonnet, A. Amy-Klein, and G. Santarelli, "Simultaneous remote transfer of accurate timing and optical frequency over a public fibre network," Appl. Phys. B **110**, 3–6 (2013).
15. B. Wang, C. Gao, W. L. Chen, J. Miao, X. Zhu, Y. Bai, J. W. Zhang, Y. Y. Feng, T. C. Li, and L. J. Wang, "Precise and continuous time and frequency synchronisation at the 5×10^{-19} accuracy level," Sci. Rep. **2**, 556 (2012)
16. F. Kefelian, O. Lopez, H. Jiang, C. Chardonnet, A. Amy-Klein, and G. Santarelli, "High resolution optical frequency dissemination on a telecommunications network with data traffic," Opt. Lett. **34**, 1573–1575 (2009).
17. O. Lopez, A. Haboucha, F. Kefelian, H. Jiang, B. Chanteau, V. Roncin, C. Chardonnet, A. Amy-Klein, and G. Santarelli, "Cascaded multiplexed optical link on a telecommunication network for frequency dissemination," Opt. Express **18**, 16849–16857 (2010).
18. P. Krehlik, Ł. Śliwczyński, Ł. Buczek, J. Kołodziej, and M. Lipiński, "ELSTAB — fibre optic time and frequency distribution technology — a general characterization and fundamental limits," IEEE Trans. Ultrason. Ferroelect. Freq. Control **63**, 993–1004 (2016).
19. O. Terra, G. Grosche, K. Predehl, R. Holzwarth, T. Legero, U. Sterr, B. Lipphardt, and H. Schnatz, "Phase coherent comparison of two optical frequency standards over 146 km using a telecommunication fibre link," Appl. Phys. B **97**, 541–551 (2009).
20. A. Pape, O. Terra, J. Friebe, M. Riedmann, T. Wubbena, E. M. Rasel, K. Predehl, T. Legero, B. Lipphardt, H. Schnatz, and G. Grosche, "Long-distance remote comparison of ultrastable optical frequencies with 10^{-15} instability in fractions of a second," Opt. Express **18**, 21477–21483 (2010).
21. S. Li, C. Wang, H. Lu, and J. Zhao, "Performance evaluation at the remote site for RF frequency dissemination over fiber," IEEE Photon. J. **9**, 7202608 (2017).
22. A. Caballero, N. Guerrero, F. Amaya, D. Zibar, and I. T. Monroy, "Long reach and enhanced power budget DWDM radio-over-fibre link supported by Raman Amplification and Coherent Detection," in *35th European Conference on Optical Communication* (2009).
23. E. K. R. Kipnoo, R. R. G. Gamatham, A. W. R. Leitch, and T. B. Gibbon, "Simultaneous signal amplification and clock distribution employing backward Raman pump over an optical fibre for applications such as square kilometer array," J. Astron. Instrum. **6**, 1750005 (2017).
24. G. M. Isoe, E. K. Rotich, and T. B. Gibbon, "VCSEL-based Raman technology for extended reach time and reference frequency transfer systems," Optoelectron. Lett. **15**, 139–143 (2019).
25. D. M. Osiemo, D. W. Waswa, K. M. Muguro, G. M. Isoe, T. B. Gibbon, and A. W. Leitch, "Modulated Raman pump for integrated VCSEL-based reach enhancement and clock tone dissemination in optical communication," Opt. Commun. **459**, 124993 (2019).
26. P. Krehlik, Ł. Śliwczyński, and Ł. Buczek, "Ultrastable long-distance fibre-optic time transfer: active compensation over a wide range of delays," Metrologia **52**, 82 (2015).
27. Ł. Śliwczyński, P. Krehlik, and Ł. Buczek, "Active propagation delay stabilization for optic frequency distribution using controlled electronic delay lines," IEEE Trans. Instrum. Meas. **60**, 1480–1488 (2011).
28. J. Ye, J. L. Peng, R. J. Jones, K. W. Holman, J. L. Hall, D. J. L. W. Hollberg, L. Robertsson, and L. S. Ma, "Delivery of high-stability optical and microwave frequency standards over an optical fiber network," J. Opt. Soc. Am. B **20**, 1459–1467 (2003).
29. B. Shillue, S. AlBanna, and L. D'Addrio, "Photonic radio-frequency dissemination via optical fiber with high-phase stability," in *Proceedings of IEEE International Topical Meeting on Microwave Photonics* (2004), p. 201.
30. G. L. Pilbratt, J. R. Riedinger, T. Passvogel, G. Crone, D. Doyle, U. Gageur, A. M. Heras, C. Jewell, L. Metcalfe, S. Ott, and M. Schmidt,

"An ESA facility for far-infrared and submillimetre astronomy," Astron. Astrophys. **518**, L1 (2010).
31. E. K. Rotich, R. G. Gamatham, A. W. R. Leitch, T. B. Gibbon, S. Malan, and H. Kriel, "MeerKAT time and frequency reference optical network: preliminary design analysis," South African J. Sci. **113**, 1–4 (2017).
32. Ł. Śliwczyński, P. Krehlik, A. Czubla, Ł. Buczek, and M. Lipiński, "Dissemination of time and RF frequency via a stabilized fibre optic link over a distance of 420 km," Metrologia **50**, 133–145 (2013).
33. W. Li, X. Zhang, and J. Yao, " Experimental demonstration of a multi-wavelength distributed feedback semiconductor laser array with an equivalent chirped grating profile based on the equivalent chirp technology," Opt. Express **21**, 19966–19971 (2013).
34. P. Q. Yang, S. Hippler, and J. Q. Zhu, "Suppressing longitudinal spatial hole burning with dual assisted phase shifts in pitch-modulated DFB lasers," Sci. China Phys. Mech. Astron. **57**, 608 (2014).
35. S. Dhoore, A. Köninger, R. Meyer, G. Roelkens, and G. Morthier, "Electronically tunable distributed feedback (DFB) laser on silicon," Laser Photon. Rev. **13**, 1800287 (2019).
36. S. T. Steger, "A fundamental approach to phase noise reduction in hybrid Si/III–V lasers," Ph.D. Thesis (California Institute of Technology, 2014).
37. T. Tadokoro, W. Kobayashi, T. Fujisawa, T. Yamanaka, and F. Kano, "High-speed modulation lasers for 100GbE applications," in *Optical Fiber Communication Conference and Exposition and the National Fiber Optic Engineers Conference (OSA/OFC/NFOEC)* (Optical Society of America, 2011), paper OWD1.
38. T. Katsuyama, "Development of semiconductor laser for optical communication," SEI Tech. Rev. **69**, 13–20 (2009).
39. H. Rong, R. Jone, A. Liu, O. Cohen, D. Hak, A. Fang, and M. Paniccia, "A continuous-wave Raman silicon laser," Nature **433**, 725–728 (2005).
40. P. K. Basu, "Silicon photonics: silicon Raman lasers," Resonance **12**, 37–46 (2007).
41. T. Honjo, T. Inoue, and K. Inoue, "Influence of light source linewidth in differential-phase-shift quantum key distribution systems," Opt. Commun. **284**, 5856–5859 (2011).
42. J. R. Vig, "Quartz crystal resonators and oscillators for frequency control and timing applications–a tutorial," in *IEEE International Frequency Control Symposium Tutorials* (2004).
43. F. L. Walls, "Phase noise issues in femtosecond lasers," Proc. SPIE **4269**, 170–177 (2001).
44. D. B. Sullivan, D. W. Allan, and F. L. Walls, "Characterization of clocks and oscillators," NIST Technical Note 1337 (U.S. GPO, 1990).
45. E. Rebeyrol, C. Macabiau, L. Ries, J.-L. Issler, and M. Bousquet, "Phase noise in GNSS transmission/reception system," in *National Technical Meeting of The Institute of Navigation*, California, January 2006, pp. 698–708.